A new shear-velocity model of continental Australia based on multi-scale surface-wave tomography: Supplementary Information

Fabrizio Magrini[1], Emanuel Kästle[2], Simone Pilia[3], Luca De Siena[1], Nicholas Rawlinson[4], and Boris Kaus[1]

[1]Institute of Geosciences, Johannes Gutenberg University, Mainz, Germany
[2]Institute for Geological Sciences, Freie Universität, Berlin, Germany
[3]College of Petroleum Engineering and Geosciences, King Fahd University of Petroleum and Minerals, Dhahran, SA
[4]Department of Earth Sciences-Bullard Labs, University of Cambridge, Cambridge, UK

May 22, 2023

This document contains:

- Statistics on the duration of the continuous seismograms employed in the ambient-noise analysis (Section 3.1 of the main text) and number of teleseismic earthquakes available per receiver pair (Section 3.2) – Fig. S1
- Illustration of our adaptive-parameterization strategy (Section 4.3), based on Love-wave velocity measurements – Fig. S2
- Depth sensitivity of Rayleigh-wave phase velocity to V_P, V_S, and ρ – Fig. S3
- Depth sensitivity of Rayleigh and Love phase velocity to V_S – Fig. S4
- Recovery test to assess the vertical resolution of our V_S model across the crust and mantle – Figs. S5 and S6
- Depth maps of Moho depth based on different iso-velocity contours – Fig. S7
- Depth maps of LAB depth based on different temperature iso-surfaces – Fig. S8

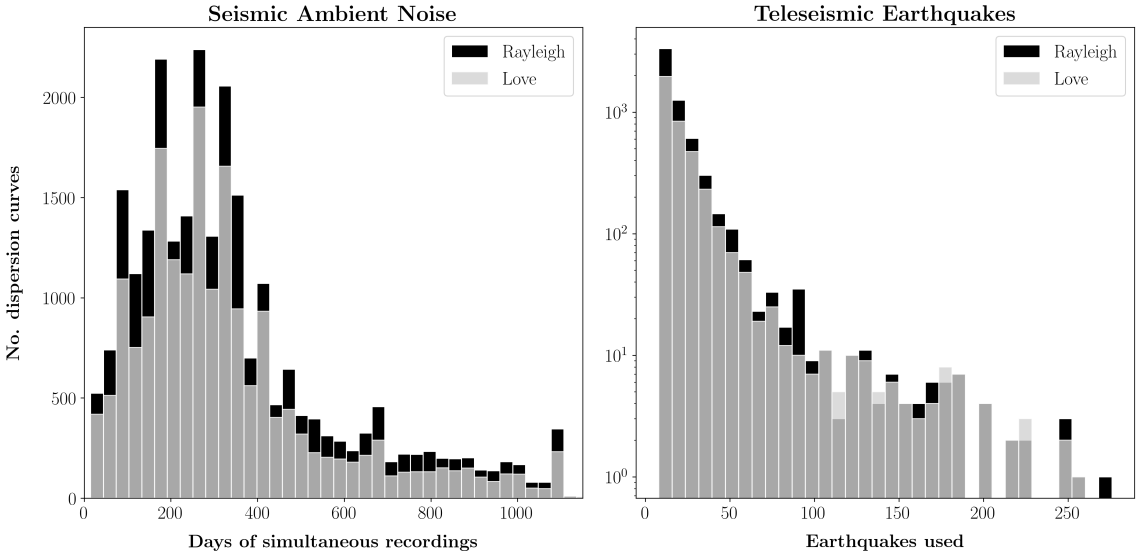

Figure S1: Histograms showing the number of days of simultaneous recordings (left) and earthquakes (right) used to calculate Rayleigh (black) and Love (gray) dispersion curves. Note the logarithmic scale on the y-axis of the right-hand side panel.

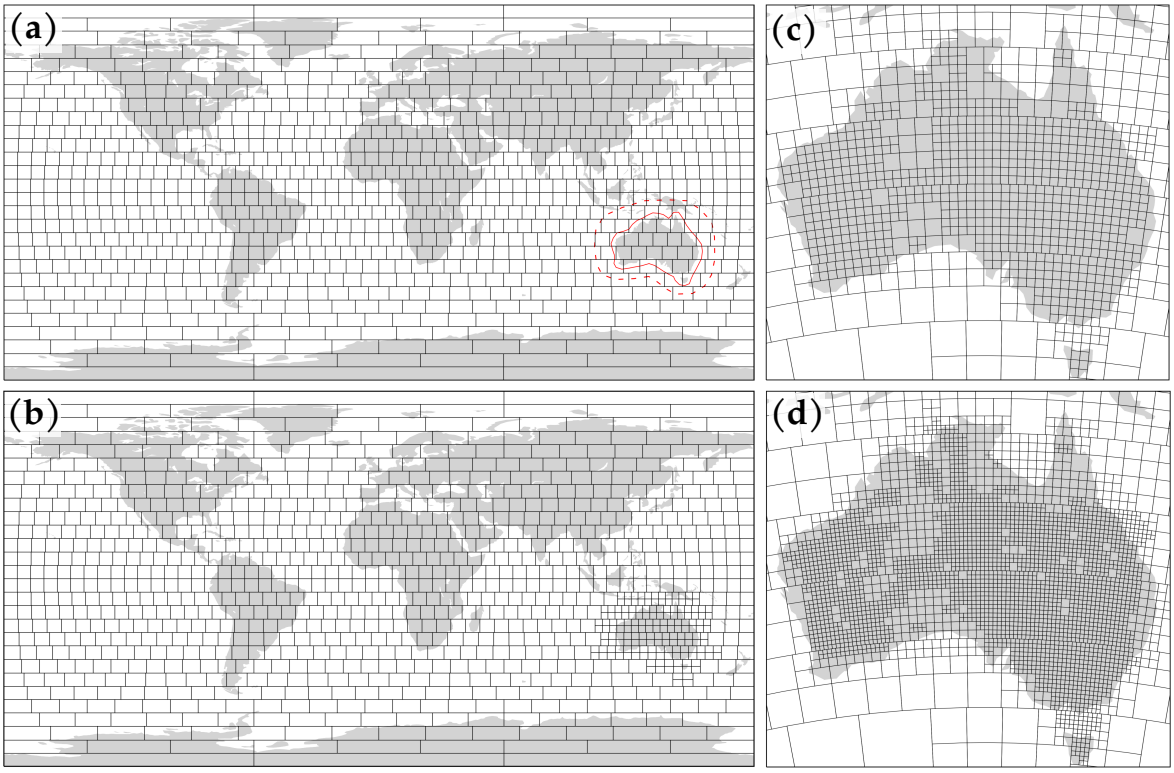

Figure S2: Similar to Fig. 4 of the main text, but obtained from Love-wave phase velocity measurements at 30 s period.

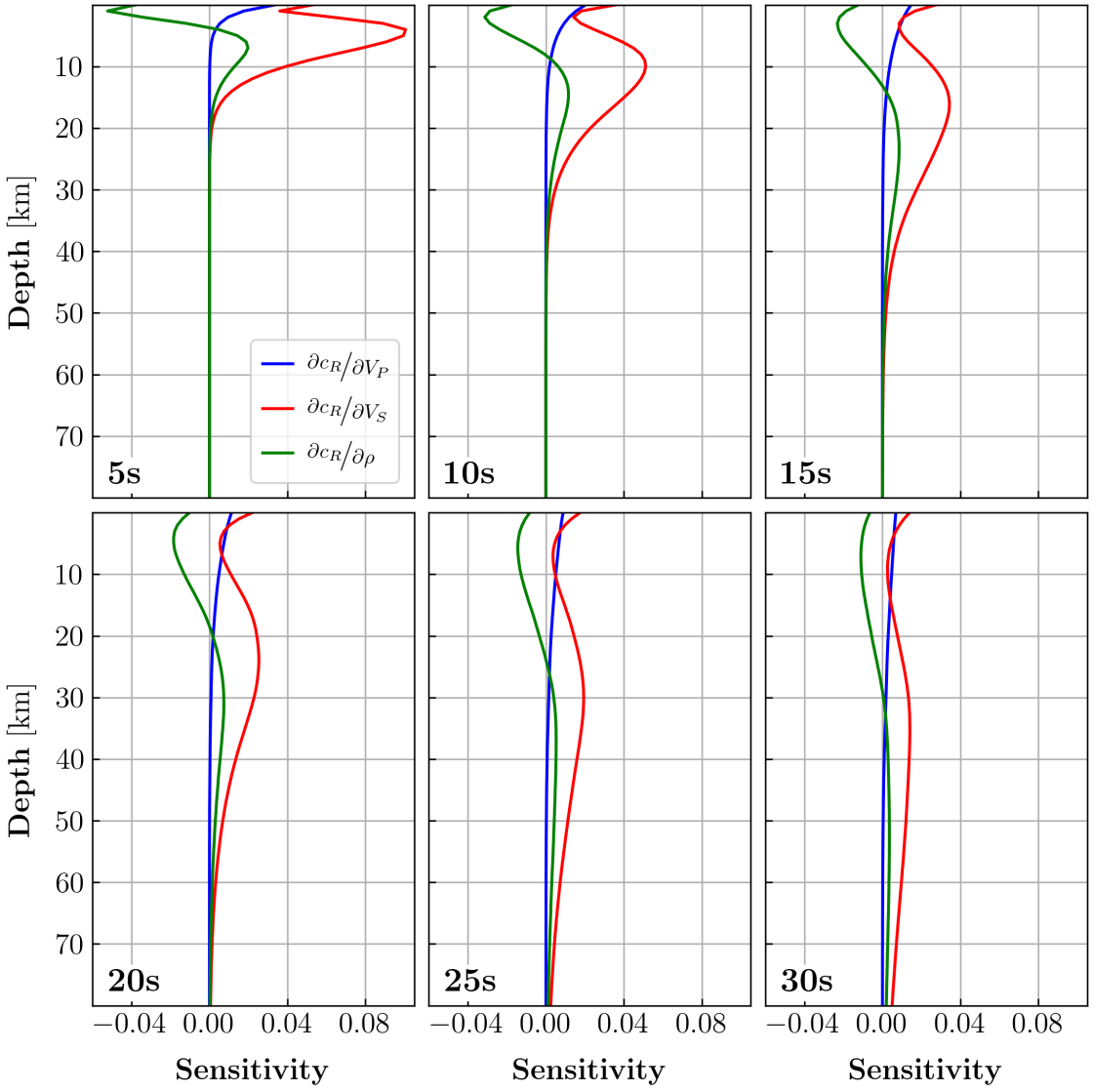

Figure S3: Depth sensitivity of Rayleigh-wave phase velocity (c_R) to V_P, V_S, and ρ at different periods (5, 10, 15, 20, 25, and 30 s). The kernels were computed from the average shear-wave velocity model retrieved in this study; for simplicity, we set $V_P = 1.8V_S$ and $\rho = 0.32V_P + 0.77$ (*Berteussen*, 1977). Note the weak sensitivity of Rayleigh waves to V_P, which decreases rapidly with increasing depth.

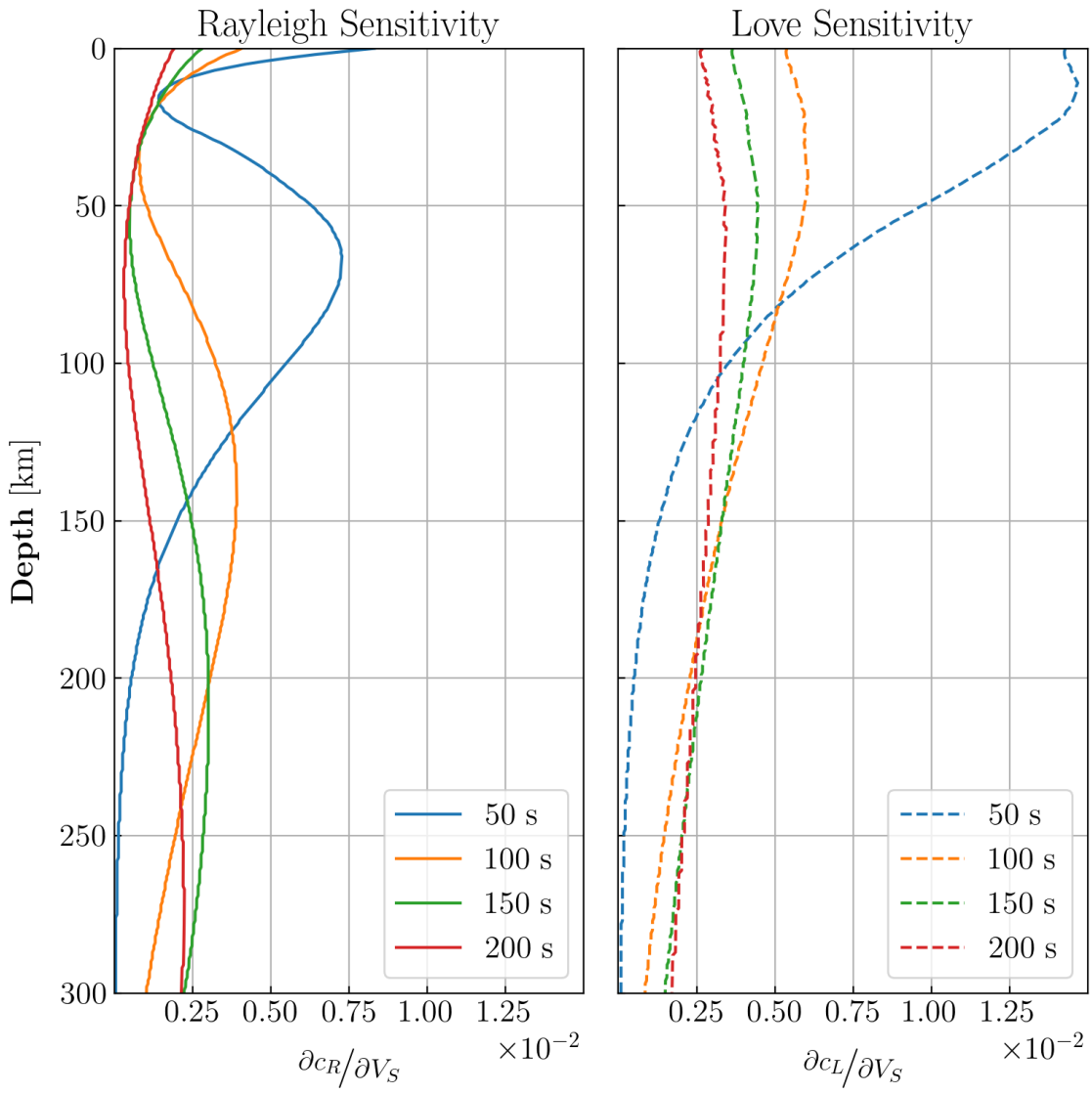

Figure S4: Depth sensitivity of Rayleigh (left) and Love (right) phase velocity to V_S at 50, 100, 150, and 200 s period. The kernels were computed as described in the caption of Fig. S3.

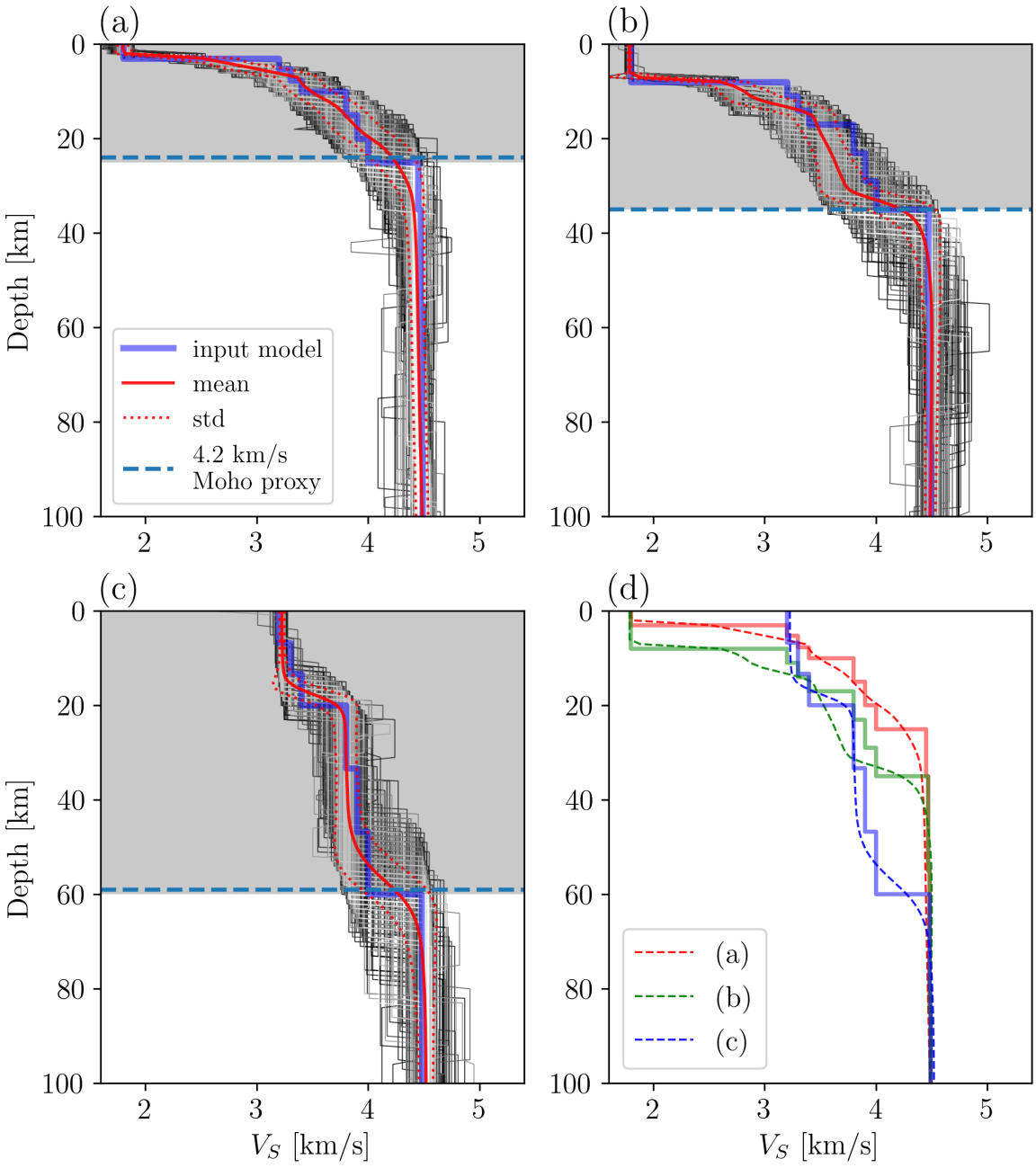

Figure S5: Recovery test to assess the resolution of our V_S model at crustal and uppermost-mantle depths. We carried out three different tests, corresponding to three different crustal models. The input model (a) has a crustal thickness of 25 km (grey-shaded area) and a 3-km-thick sedimentary layer. Model (b) has a crustal thickness of 35 km and an 8-km-thick sedimentary layer. Model (c) has no sedimentary layer and a crustal thickness of 60 km. We used each of these models (blue lines) to generate synthetic observations of Rayleigh and Love phase velocity, which we subsequently inverted for V_S as explained in Section 5. In each panel, the retrieved models (red lines) are shown along with the synthetic input. Panel (d) displays the three synthetic and retrieved models together. Based on this test, we infer that our inversion scheme is able to capture crustal variations in V_S at relatively high resolution. Absolute velocities and relative variations between different models are well constrained.

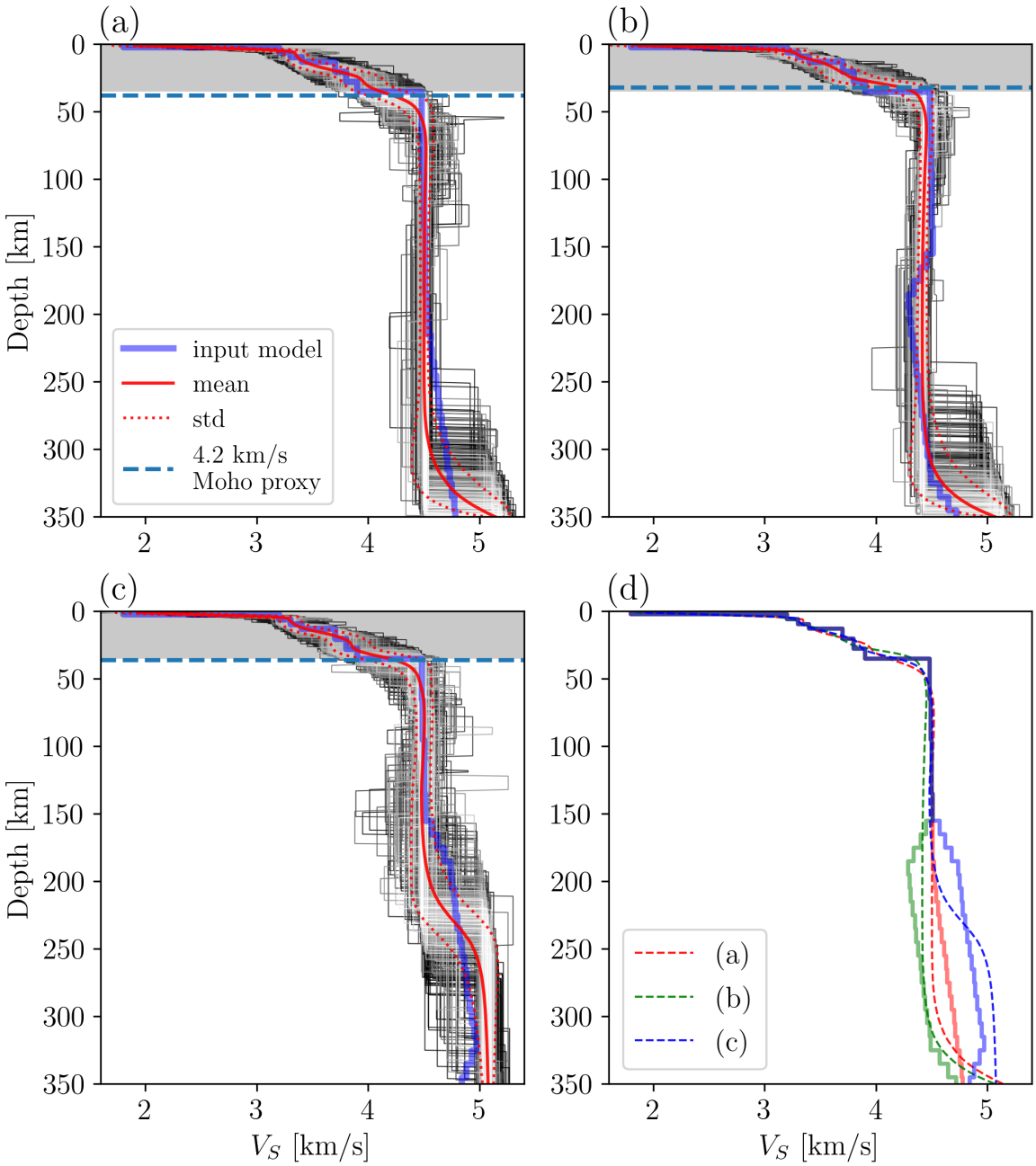

Figure S6: Similar to Fig. S5, but obtained from different mantle models. In panel (a), we carried out a synthetic test to recover the V_S structure of IASP91 (blue line, *Kennet*, 1991). The input models in panels (b) and (c) were obtained by perturbing (a) at depths greater than 150 km, resulting in relatively slow and fast mantle anomalies (±5%). The retrieved models (red lines) faithfully reproduce the synthetic inputs at depths above 150 km. At greater depths, our data set of fundamental-mode surface waves cannot capture abrupt velocity variations (see panels b and c). Nonetheless, as shown in panel (d), our data set is able to discriminate between relatively slow and fast mantle. This provides confidence in the lateral variations in V_S (and therefore in those of our LAB proxy) discussed in the main text.

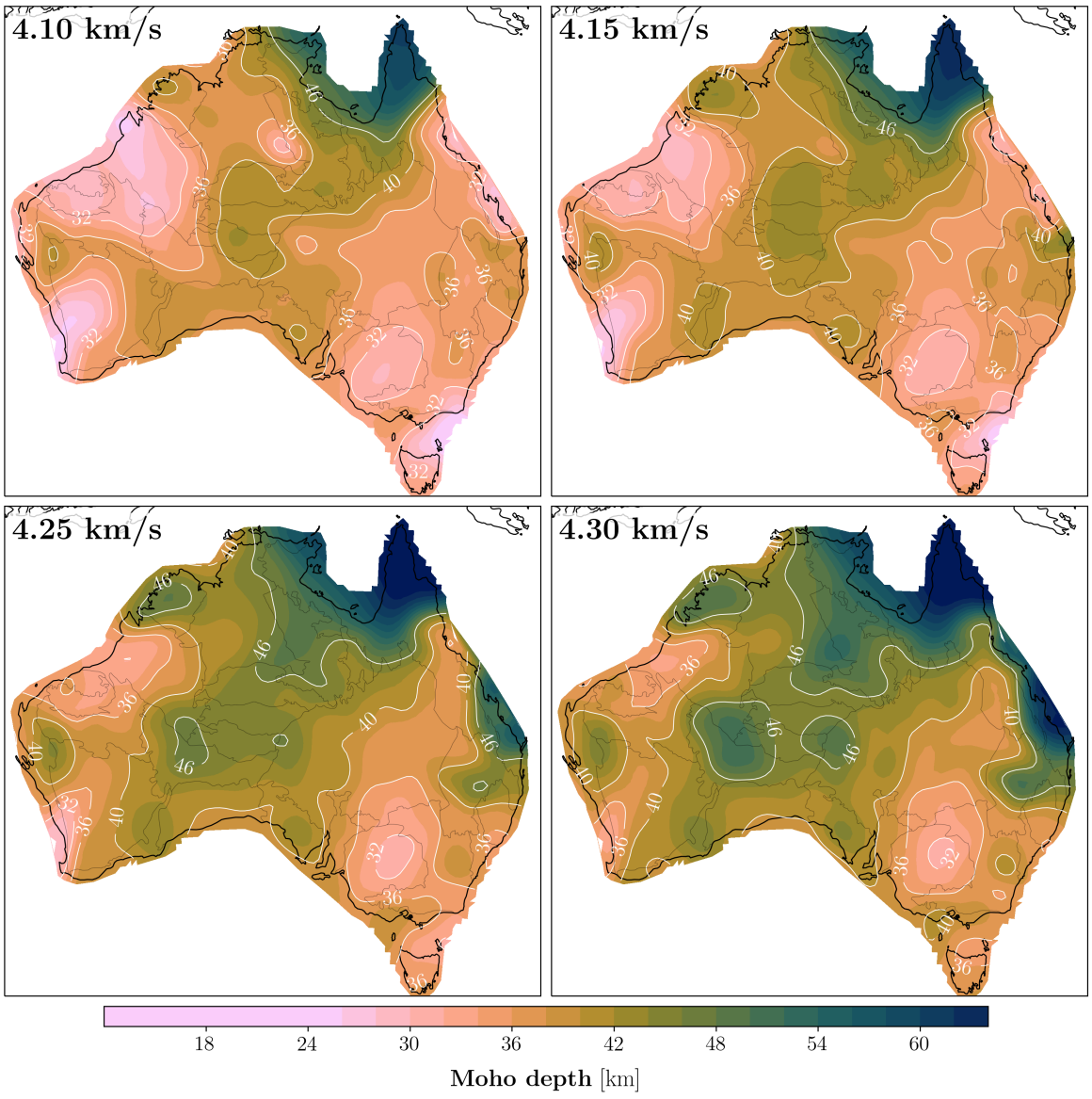

Figure S7: Moho-depth maps as obtained from iso-velocity contours of our V_S model at 4.1, 4.15, 4.25, and 4.3 km/s. While different contour choices result in non-negligible variations in the retrieved crustal thicknesses, they do not undermine the larger scale spatial patterns of Moho depth (see Section 6.1.3 of the main text).

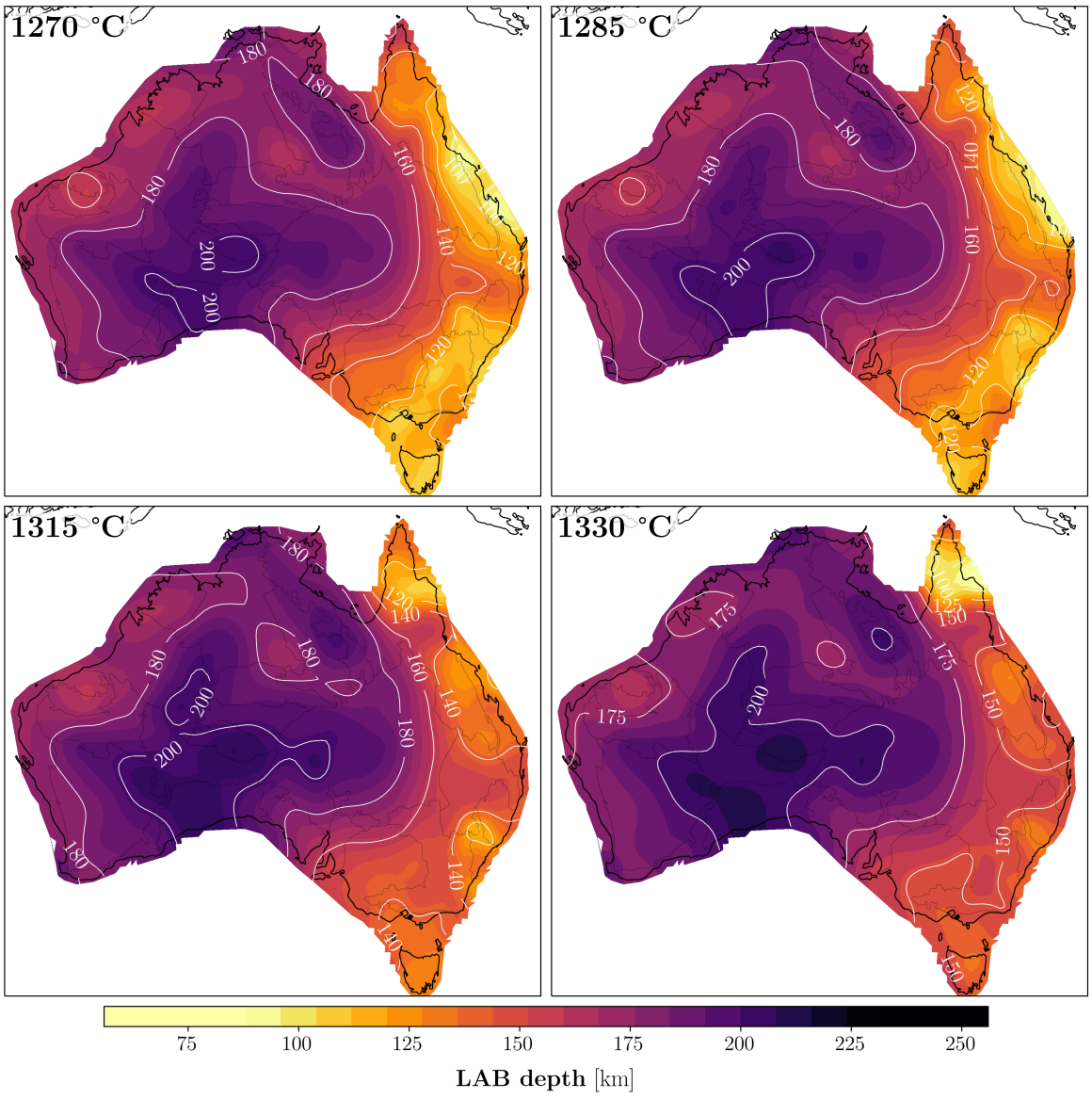

Figure S8: Depth maps of LAB as obtained by considering different temperature iso-surfaces (1270, 1285, 1315, and 1330 °C). Similar to Fig. S7, different temperature choices result in non-negligible differences in the estimates of lithospheric thickness, but do not mask the larger scale spatial patterns (see Section 6.2.1 of the main text).

References

Berteussen, K.-A., Moho depth determinations based on spectral-ratio analysis of NORSAR long-period P waves, *Physics of the Earth and Planetary Interiors*, *15*(1), 13–27, 1977.

Kennet, B., IASPEI 1991 seismological tables, *Terra Nova*, *3*(2), 122–122, https://doi.org/10.1111/j.1365-3121.1991.tb00863.x, 1991.